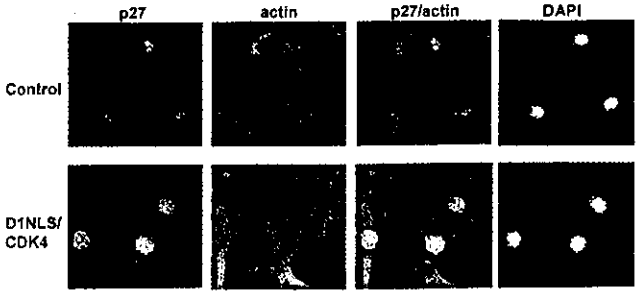

FIG. 2. **p27 accumulated in the nuclei of cardiomyocytes after cell cycle entry by D1NLS/CDK4.** Control untreated and D1NLS/CDK4 cells at 48 h post-infection were fixed and stained for p27 (*green*) and sarcomeric actin (*red*) with anti-p27 and anti-sarcomeric actin antibodies, respectively, as described under "Experimental Procedures." Cell nuclei (*white*) were also stained with 4',6-diamidino-2-phenylindole (*DAPI*).

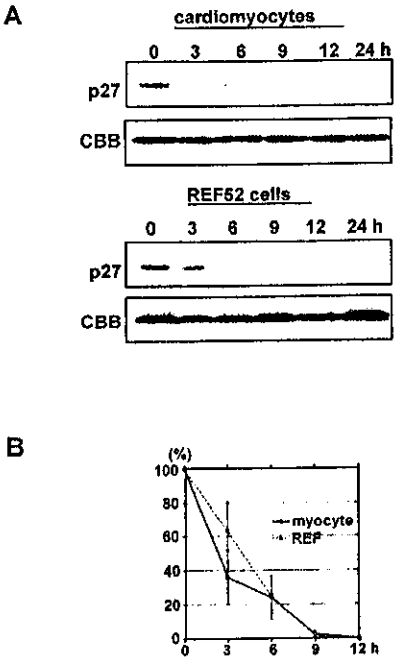

FIG. 3. **Serum-induced degradation of p27 in cardiomyocytes was not different from REF52 cells.** *A*, cardiomyocytes and REF52 cells were serum-starved for 48 h and then treated with serum (10% fetal bovine serum). At each time after adding the serum, cell extract (20 μg) was assayed for p27 by Western blot analysis. *Lower panels* show the Coomassie Brilliant Blue (*CBB*) staining as the control for protein loading. In *B*, the amount of p27 protein was quantitated by densitometric measurement and expressed as percent of that at time 0. Results represent the mean ± S.E. three independent experiments.

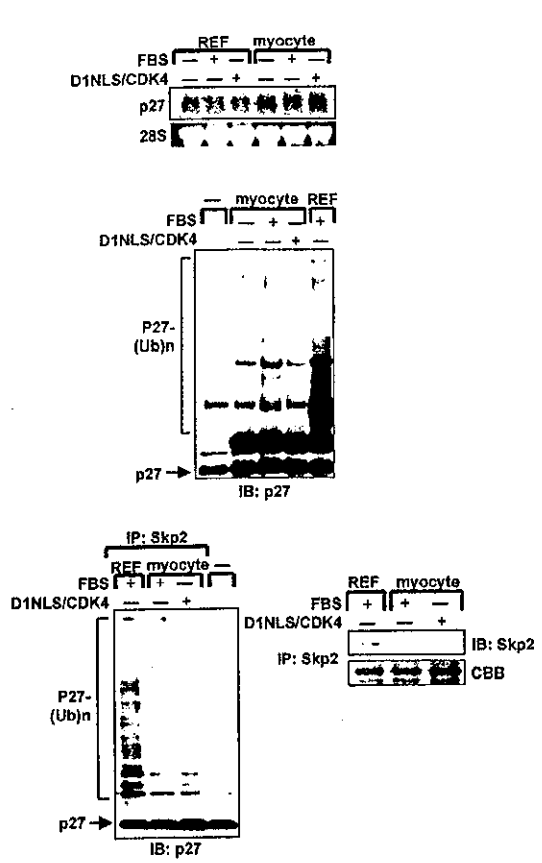

FIG. 4. **Cardiomyocytes showed the impaired Skp2-dependent degradation of p27.** *A*, total RNA (10 μg) from the control, serum, or D1NLS/CDK4-treated cardiomyocytes and REF52 cells was analyzed for p27 mRNA by Northern blot analysis as described under "Experimental Procedures." *B*, equal amounts of cell extract (50 μg of protein) treated as in *A* were assayed for the *in vitro* p27 ubiquitylation activity as described under "Experimental Procedures." *C*, cell extracts (50 μg of protein) from cells treated as in *B* were immunoprecipitated with anti-Skp2 antibody and the resulting complexes were assayed for the Skp2 protein (*right panel*) and the *in vitro* p27 ubiquitylation activity (*left panel*), respectively. *CBB*, Coomassie Brilliant Blue; *FBS*, fetal bovine serum.

assay using anti-72K antibody. Cardiomyocytes were infected at the indicated multiplicity of infection in serum-free minimal essential medium for 60 min with brief agitation every 15 min, and then the medium was replaced with culture medium.

Construction of Adenovirus Vector Encoding p27 SiRNA—Oligonucleotides for expressing stem-loop RNAs that target three different regions of rat *p27* were ligated with human U6 promoter and the resulting transcription unit of the U6 promoter was subcloned into the SwaI site of the E1-deleted region of cassette cosmid vector pAxcw (Adenovirus Expression Vector Kit, TaKaRa BIO). Adenoviral vector was then prepared as in the protocol from Takaka. Oligonucleotide sequences used were: 5'-CACCGGTAGGAGGTTCTTCTTCAACGTGTGCTGTCCGTTGAAGAAGAATCTTCTGCCTTTTT-3' and 5'-GCATAAAAGGCAGAAGATTCTTCTTCAACGGACAGCACACGTTGAAGAAGAACCTCCTACC-3' (#1) for the p27 amino acid region from 830 to 848, 5'-CACCAGTGTAAGTGGAGTTTCGAACGTGTGCTGTCCGTTCGAAATTCCACTTGCGCTTTTTT-3' and 5'-GCATAAAAAAGCGCAAGTGGAATTTCGAACGGACAGCACACGTTCGAAACTCCACTTACACT-3' (#4) from 532 to 550, or 5'-CACCGTGGGAGTGTTTAATGGGAACGTGTGCTGTCCGTTCCCGTTAGACACTCTCACTTTTT-3' and 5'-GCATAAAAAGTGAGAGTGTCTAACGGGAACGGACAGCACACGTTCCCATTAAACACTCCCAC-3' (#6) from 372 to 390, respectively. Adenovirus vector encoding siRNA for hepatitis C viral protein (siRNA331) was as described (24) and employed as control.

Whole Cell Extract Preparation and Western Blot Analysis—Cardiomyocytes (2×10^6 cells) treated as indicated were washed in phosphate-buffered saline, resuspended in 50 μl of lysis buffer (50 mM Hepes-KOH, pH 7.6, 150 mM NaCl, 1% Tween 20, 10 mM glycerophosphate, 2.5 mM EGTA, 1 mM EDTA, 0.1 mM phenylmethylsulfonyl fluoride, 10 μg/ml each leupeptin and aprotinin, 0.1 mM sodium vanadate, 1 mM NaF, and 10% glycerol), and incubated on ice for 30 min. After centrifugation at 12,000 rpm for 10 min, whole cell extract was obtained. The amount of protein was measured with the Lowry method using bovine serum albumin as standard. Whole cell extracts (usually 20 μg of protein) were separated by SDS-PAGE, transferred onto an Immobilon-P membrane (Millipore), and subjected to Western blot using the protocol of the ECL kit (Amersham Biosciences) as described (20).

Immunoprecipitation and Kinase Assays—Whole cell extracts (50 μg of protein) were immunoprecipitated with anti-CDK4 (0.4 μg) or anti-CDK2 antibody (0.4 μg) followed by Western blot with the indicated antibody, and bands were detected using monoclonal anti-rabbit IgG (γ-chain specific) peroxidase-conjugated secondary antibody (Sigma). To assay CDK4 and CDK2 kinase activity, the immunoprecipitated complexes were incubated with glutathione *S*-transferase-Rb and histone H1, respectively, as substrates as described (10, 22).

RNA Isolation and Northern Blot Analysis—Total RNA was isolated by the acid-guanidium method using Isogen (Nippon Gene, Japan),

fractionated on a formaldehyde/agarose gel, transferred to a Hybond-N membrane, and hybridized to random-primed cDNA probes for the mouse *p27* and *skp2* genes as described (22). The membrane was exposed and analyzed with a Bas 2500 Bioimage analyzer (Fujifilm Co., Tokyo, Japan). DNA fragments (100 ng) for these cDNAs were radiolabeled with 50 μCi of [α-^{32}P]dCTP (6000 Ci/mmol, Amersham Biosciences) using a random primer labeling kit from Takara and used as probe for RNA preparation and Northern blot analysis.

In Vitro Ubiquitylation Assay—Cells were treated in lysis buffer (20 mM Hepes-KOH, 0.42 M NaCl, 1.5 mM $MgCl_2$, 0.2 mM EDTA, 0.5% Nonidet P-40, 0.1 mM phenylmethylsulfonyl fluoride, 10 μg/ml each leupeptin and aprotinin, and 25% glycerol) on ice for 30 min, and cell debris was removed by centrifugation at 15,000 rpm for 20 min. Cell extract (50 μg of protein) was incubated with substrates in 15 μl of buffer of 40 mM Hepes-NaOH (pH 7.9), 60 mM potassium acetate, 2 mM dithiothreitol, 5 mM $MgCl_2$, 0.5 mM EDTA, 10% glycerol, and 1.5 mM ATP containing 50 ng of Uba1, 100 ng of UbcH5A, 3 μg of glutathione *S*-transferase-ubiquitin. After incubating at 26 °C for 30 min, reaction products were separated by SDS-PAGE and analyzed by Western blot with the indicated antibody. As substrates, FLAG-p27 or -Skp2 were prepared using 1 μg of pcDNA3Flag-p27 or pcDNA3Flag-skp2 (23) and 25 μl of rabbit reticulocyte lysate (TNT kit from Promega) according to its protocol. The *in vitro* p27 ubiquitylation activity was also assayed after immunoprecipitation of cell extracts with 0.4 μg of anti-Skp2 antibody.

Immunocytological Study and Cell Cycle Analysis—To examine the expression of p27 in cardiomyocytes, cells grown on glass coverslips were fixed in 70% ethanol, double-stained with anti-p27 and anti-sarcomeric actin antibodies, and visualized using fluorescent tyramide reagent according to the manufacturer's protocols (TSA-direct NEL-701, PerkinElmer Life Sciences, Inc.). Confocal images were obtained using the laser-scanning confocal image system (LSM510, Zeiss). For cell cycle analysis, cells were stained with anti-sarcomeric actin and anti-mouse antibodies conjugated with fluorescein isothiocyanate (23799, Polysciences), followed by treatment with propidium iodide (50 μg/ml) and RNase A (500 μg/ml). The DNA content of cells positive for sarcomeric actin was analyzed using a laser scanning cytometer (LSC 101, Olympus).

Statistical Analysis—Quantitative data were expressed as mean ± S.E. Statistical analysis was performed with the Student's *t* test.

RESULTS

CDK2 Activity Was Suppressed and the Cell Cycle Inhibitor p27 Accumulated in the Nuclei of Cardiomocytes after Cell Cycle Entry by D1NLS/CDK4—We have previously shown that D1NLS/CDK4 expression allowed the cardiomyocytes to enter the cell cycle (10). However, the proliferation of these cells was limited to approximately one or two cycles. To understand the mechanism by which the cells cease to proliferate, we first assayed the activity of G_1 cyclin kinase, CDK4 and CDK2. As shown in Fig. 1*A*, the CDK4 activity was up-regulated at 24 h post-infection of D1NLS/CDK4, and remained active for at least 96 h. The CDK2 activity was also activated at 24 h, but suppressed again at 48 h, whereas the amount of CDK2 was not significantly affected. We, therefore, examined the expression of CDK2 inhibitors, p27 and p21. Fig 1*B* showed that p27 was accumulated in the serum-starved non-proliferating cardiomyocytes. When these cells were allowed to enter the cell cycle by D1NLS/CDK4, the p27 protein was rapidly degraded within 24 h. However, it accumulated again at 48 h, at which time CDK2 was inhibited (Fig. 1*A*). In REF52 fibroblasts, p27 was also rapidly degraded after entering the cell cycle by D1NLS/CDK4, but no accumulation was observed for at least 72 h. The expression of p21 was significantly suppressed in serum-starved cardiomyocytes and REF52 cells, but up-regulated at 48 h after the cell cycle entry. In Fig. 1*C*, immunoprecipitaion of the cardiomyocyte extract was performed using anti-CDK2 antibody. Results showed that p27 was little associated with CDK2 in the serum-starved cells, but the higher amount of p27 was detected in the CDK2 complex at 48–96 h. In contrast, appreciable amounts of p21 were not detected in the CDK2 complex. It was further noted that the expression of p57 and p53, other cell cycle inhibitors, was not significantly altered in D1NLS/CDK4 cells of this study (data not shown).

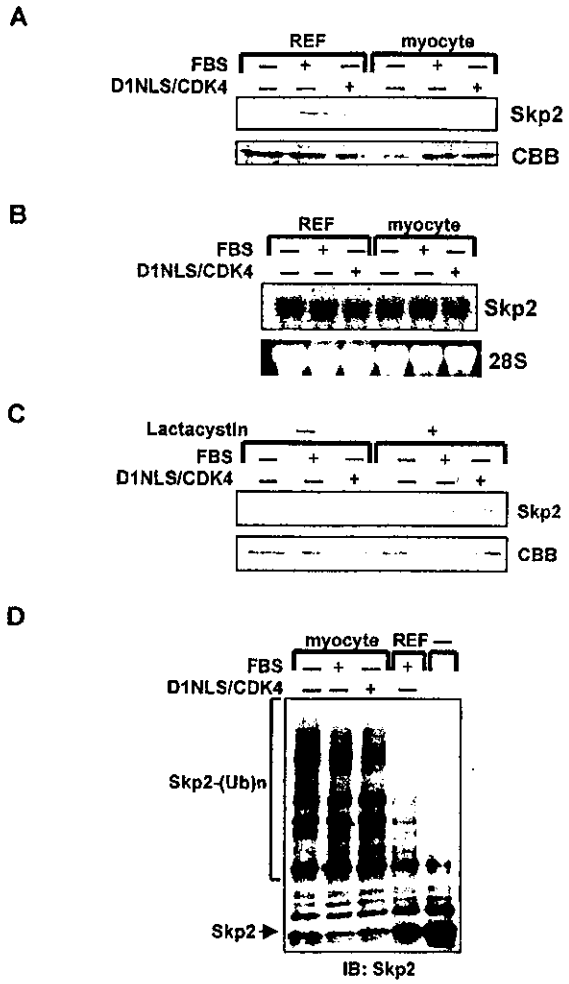

FIG. 5. **Down-regulation of Skp2 was inversely correlated to the *in vitro* Skp2 ubiquitylation activity in cardiomyocytes.** *A*, cardiomyocytes and REF52 cells were treated with serum (10% FBS) or D1NLS/CDK4 for 48 h, and their cell extracts (20 μg of protein) were assayed for Skp2 protein by Western blot analysis. *B*, cardiomyocytes and REF52 cells were treated as in *A*, and their total RNA (10 μg) was analyzed for Skp2 mRNA by Northern blot. *C*, cells were treated as in *A* in the presence or absence of 20 μM lactacystin, and their cell extracts were assayed for Skp2 protein by Western blot analysis. *Lower panels* show the Coomassie Brilliant Blue (*CBB*) staining as control for protein loading. *D*, cell extracts (50 μg of protein) were assayed for the *in vitro* Skp2 ubiquitylation activity as described under "Experimental Procedures." *IB*, immunoblot.

Next, the immunocytological study of p27 expression was performed. As shown in Fig. 2, p27 accumulated significantly in the nuclei of D1NLS/CDK4 cells, whereas its expression was little detected in control cells. These data altogether indicated that the p27 protein was degraded after initiation of cell cycle, but was accumulated again in the nuclei during cell cycle progression of cardiomyocytes.

Serum-induced Degradation of p27 in Cardiomyocytes Was Not Different from REF52 Cells—The protein level of p27 is predominantly controlled by the rate of degradation through the proteasome-dependent pathway. This degradation is mediated by the Skp2-independent ubiquitin ligase in the cytoplasm at G_0 to G_1 transition and by the Skp2-dependent ligase in the nuclei at S to G_2 phase, respectively (12, 17–19). In Fig. 3*A*, p27 accumulated when the cardiomyocytes and REF52 cells were serum-starved. We stimulated these cells with serum and the degradation of p27 was determined by Western blot analysis. Results showed that p27 was degraded in both cell types with

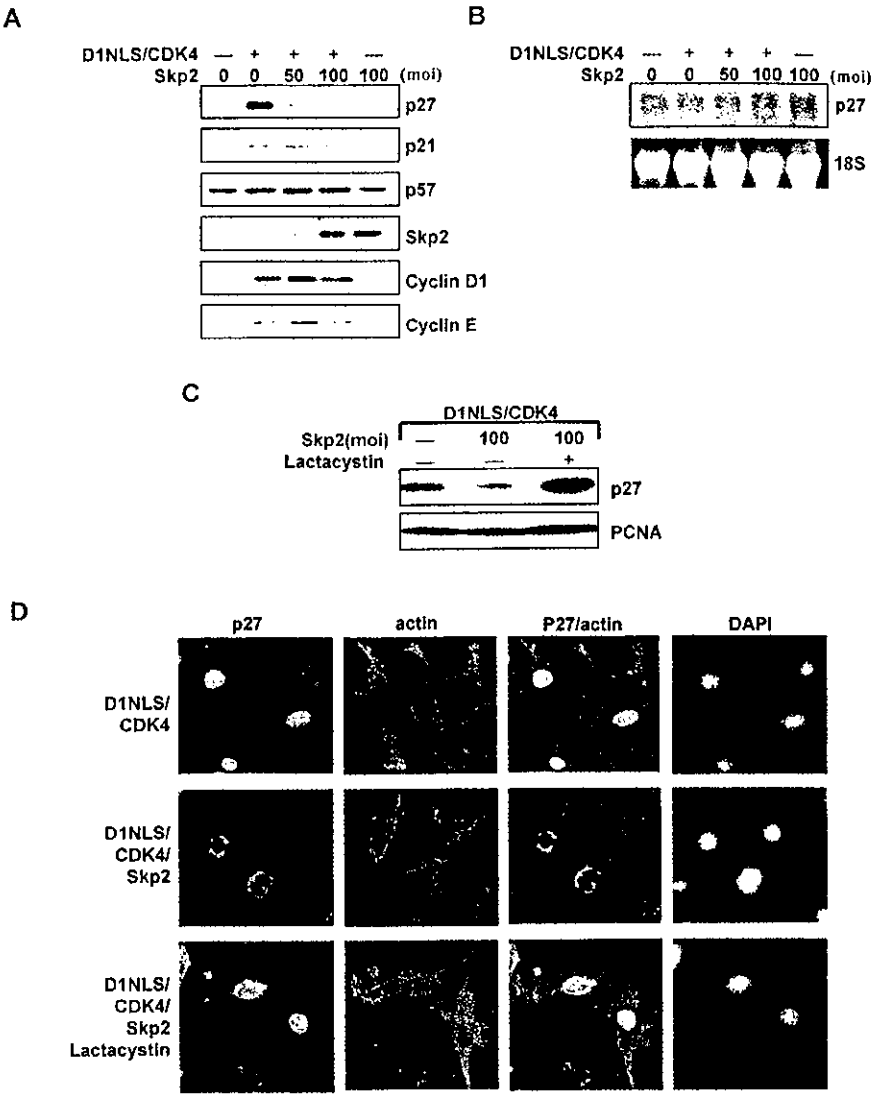

FIG. 6. **Skp2 expression caused a specific degradation of p27 in nuclei of D1NLS/CDK4 cardiomyocytes.** *A*, cardiomyocytes were infected with a combination of AdD1NLS/AdCDK4 and an increasing multiplicity of infection of Ad-Skp2. At 48 h post-infection, cell extracts (20 μg of protein) were prepared and assayed for various cell cycle regulators by Western blot analysis. *B*, total RNA (10 μg) was assayed for p27 mRNA as described in the legend to Fig. 3*A*. *C*, cardiomyocytes were treated as in *A* in the presence or absence of 20 μM lactacystin, and their extract (20 μg of protein) was assayed for p27 protein. Proliferating cell nuclear antigen (*PCNA*) was shown as a loading control. *D*, D1NLS/CDK4 and D1NLS/CDK4/Skp2 cardiomyocytes with or without 20 μM lactacystin treatment were immunostained for p27 with anti-p27 antibody. Sarcomeric actin and cell nuclei were also stained with anti-sarcomeric actin antibody and 4',6-diamidino-2-phenylindole (*DAPI*), respectively (*green*, p27; *red*, sarcomeric-actin; *white*, DAPI).

apparently similar kinetics (Fig. 3*B*). This strongly indicates that there is no apparent difference of p27 degradation between the cardiomyocytes and proliferating REF52 cells during their transition from G_0 to G_1 phase, although cardiac cells are not allowed to enter the cell cycle by serum treatment.

Skp2-dependent Degradation of p27 Was Suppressed in Cardiomyocytes—We next examined the p27 expression of cardiomyocytes after their entry into the cell cycle by D1NLS/CDK4 expression. The p27 mRNA level in cardiomyocytes was comparable with that of REF52 cells and unaltered by serum treatment or expression of D1NLS/CDK4 (Fig. 4*A*). We next examined p27 degradation by assaying the *in vitro* ubiquitylation activity. Fig. 4*B* showed that the p27 protein was highly ubiquitylated and migrated as a multiubiquitylated form when assayed using cell extract from REF52 cells. In contrast, the extracts from the control, serum-stimulated or D1NLS/CDK4-infected cardiomyocytes exhibited the lower activity compared with REF52 cells. We next examined the Skp2-dependent degradation of p27 after immunoprecipitating the Skp2-ligase complex. As shown in Fig. 4*C*, *left panel*, cardiomyocytes contained only marginal activity of p27 ubiquitylation, whereas REF52 cells exhibited significant activity. Under this condition, the complex from REF52 cells contained the higher amount of Skp2 protein than the cardiomyocytes (Fig. 4*C*, *right panel*). From these data, it is indicated that cardiomyocytes have much lower activity of Skp2-dependent p27 degradation than the growing REF52 cells.

Skp2 Protein Was Down-regulated through Its Accelerated Degradation in Cardiomyocytes—The data above strongly suggested that the impaired degradation of p27 by Skp2 might cause p27 accumulation during cell cycle progression of cardiomyocytes. We, therefore, examined the expression of Skp2 in cardiomyocytes. As shown in Fig. 5*A*, Skp2 protein was detected in the serum-starved REF52 cells, and it was induced after treatment with serum or D1NLS/CDK4. In cardiomyocytes, however, Skp2 expression was hardly detected or significantly suppressed in the serum-starved cardiac cells, and no significant induction was observed by serum or D1NLS/CDK4. Northern blot analysis revealed that apparently similar amounts of Skp2 mRNA was expressed in both cell types under these conditions (Fig. 5*B*). When these cardiomyocytes were treated with lactacystin, a proteasome inhibitor, Skp2 protein was remarkably stabilized (Fig. 5*C*), indicating that Skp2 protein was expressed but actively degraded in cardiomyocytes. Therefore, we further measured the *in vitro* ubiquitylation activity of Skp2 protein. Fig. 5*D* revealed that Skp2 protein was actively ubiquitylated and migrated as the multiubiquitylated products when assayed using extracts from cardiomyo-

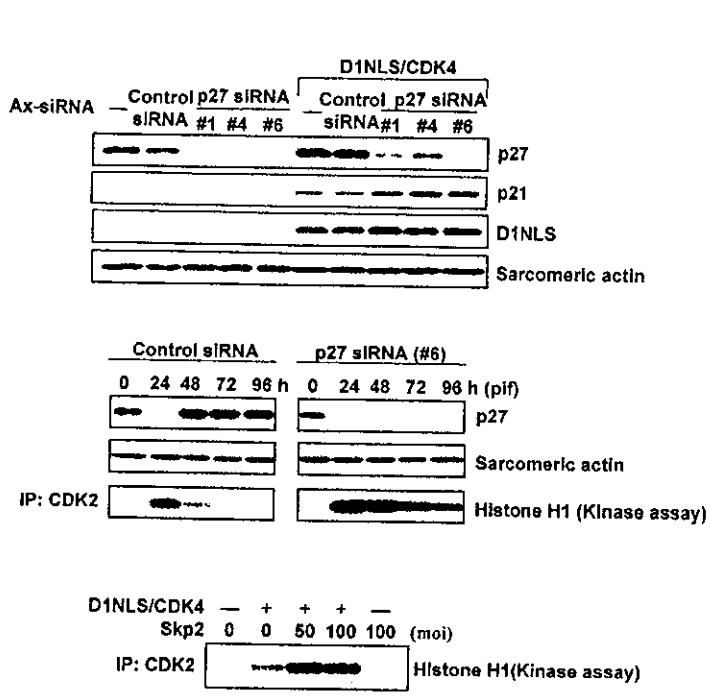

FIG. 7. **Specific down-regulation of p27 by siRNA or Skp2 abrogated early suppression of CDK2 activity in D1NLS/CDK4 cells.** *A*, cardiomyocytes were untreated or infected with a combination of AdD1NLS/AdCDK4 and adenovirus vectors encoding p27 siRNA 1, 4, 6, or hepatitis C viral protein (control). At 48 h post-infection, cell extracts (20 μg of protein) were prepared and assayed for p27, p21, and cyclin D1 by Western blot analysis. Sarcomeric actin was shown as control for protein loading. *B*, cells were infected with a combination of AdD1NLS/AdCDK4 and virus vector for control siRNA or p27 siRNA (*#6*). At the indicated time, cell extracts (20 μg) were assayed for p27 and CDK2 kinase (*Histone H1 kinase*) activity as described under "Experimental Procedures." *C*, cells were infected with a combination of AdD1NLS/AdCDK4 and an increasing multiplicity of infection of AdSkp2, and after 48 h, CDK2 activity was assayed as in *B*.

cytes, and this activity appeared not to be affected by serum or D1NLS/CDK4 treatment. In contrast, the activity was significantly suppressed in growing REF52 cells. This demonstrated that Skp2 degradation was highly activated in cardiomyoctes, and this was inversely correlated to the Skp2-dependent p27 degradation (Fig. 4*C*). From these results, it is indicated that the Skp2 protein is actively degraded in cardiomyocytes, possibly because of their increased Skp2 ubiquitylation, and this may in turn lead to the accumulation of the p27 protein.

Overexpression of Skp2 Caused Specific Degradation of p27—We next examined whether the down-regulation of Skp2 protein is functionally linked to accumulation of p27 in D1NLS/CDK4 cardiomyocytes. For this purpose, the Skp2 protein was overexpressed using the adenovirus-mediated gene transfer. As shown in Fig. 6*A*, the expression of Skp2 caused the significant degradation of p27 in D1NLS/CDK4 cells. In contrast, p21, p57, and cyclin D1 and E were only marginally affected. The p27 mRNA level was only slightly induced by Skp2 expression (Fig. 6*B*). Furthermore, the decrease of p27 by Skp2 expression was abrogated by lactacystin treatment (Fig. 6*C*), indicating that down-regulation of the p27 protein was specifically mediated by the Skp2-dependent degradation. Immunocytological study revealed that the accumulation of the p27 protein in the nuclei of D1NLS/CDK4 cardiomyocytes was significantly suppressed by Skp2 expression, and this suppression was inhibited by lactacystin treatment (Fig. 6*D*). These data altogether indicated that Skp2 enhanced the specific degradation of p27 in the nuclei of D1NLS/CDK4 cardiomyocytes through a proteasome-dependent pathway.

Down-regulation of p27 by siRNA or Skp2 Stimulated the CDK2 Activity and Overrode the Limited Cell Cycle Progression of D1NLS/CDK4 Cardiomyocytes—We further addressed whether the accumulation of p27 had a causal effect on the early cell cycle arrest of D1NLS/CDK4-infected cardiomyocytes. For this purpose, we employed a loss-of-function approach by an RNA interference-mediated gene knockdown. As shown in Fig. 7*A*, three vectors expressing different p27 siRNAs specifically caused the knockdown of p27 protein in both control and D1NLS/CDK4 cells, whereas they showed no inhibition of another CDK inhibitor p21. Next, we measured the p27 protein and CDK2 activity in D1NLS/CDK4 cells expressing these siRNAs. Fig. 7*B* showed that the suppression of CDK2 activity was totally abrogated when the re-accumulation of p27 was knocked down by p27 siRNA. By contrast, in cells expressing control siRNA, p27 was re-accumulated and CDK2 activity was suppressed as in D1NLS/CDK4 cells (compare with Fig. 1). The p27 degradation by Skp2 also prevented the suppression of CDK2 activity in D1NLS/CDK4 cells (Fig. 7*C*). These data strongly indicated that p27 played a major role in suppressing CDK2 activity in D1NLS/CDK4 cells.

Based on these results, we next measured cell cycle progression and proliferation by p27 siRNA or Skp2. Fig. 8*A* showed that a higher proportion of the D1NLS/CDK4/p27 siRNA or D1NLS/CDK4/Skp2 cells progressed to S/G_2M phase much faster than the D1NLS/CDK4 cells. Furthermore, these cells still retained the higher proportion of S/G_2/M cells at 192 h post-infection, compared with control D1NLS/CDK4 cells. When the cell number was counted, it was shown that p27 siRNA or Skp2 further promoted the proliferation of D1NLS/CDK4 cells (Fig. 8*B*). The apparent doubling time of cell proliferation was 64, 63.6, and 84 h for the D1NLS/CDK4/p27 siRNA, D1NLS/CDK4/Skp2, and D1NLS/CDK4 cells, respectively. By contrast, p27 siRNA or Skp2 expression alone had no significant effect. Therefore, it is indicated that down-regulation of p27 enhanced further stimulation of CDK2 activity and subsequent cell cycle progression of D1NLS/CDK4 cells.

DISCUSSION

In the present study, we demonstrated that the accumulation of CDK inhibitor p27 was a strong barrier of cell cycle in terminally differentiated cardiomyocytes, and this was caused, at least in part, by the impaired Skp2-dependent p27 degradation in the nuclei of cells.

p27 is degraded at least in two phases of the cell cycle. When cells transit from the G_0 to G_1 phase in response to growth stimuli such as serum, p27 is degraded in the cytoplasm by the Skp2-independent pathway. On the other hand, in proliferating cells, p27 is degraded in the nuclei during S and G_2 phase by a Skp2-dependent pathway (17, 19). The impaired Skp2-dependent nuclear degradation of p27 in cardiomyocytes is sup-

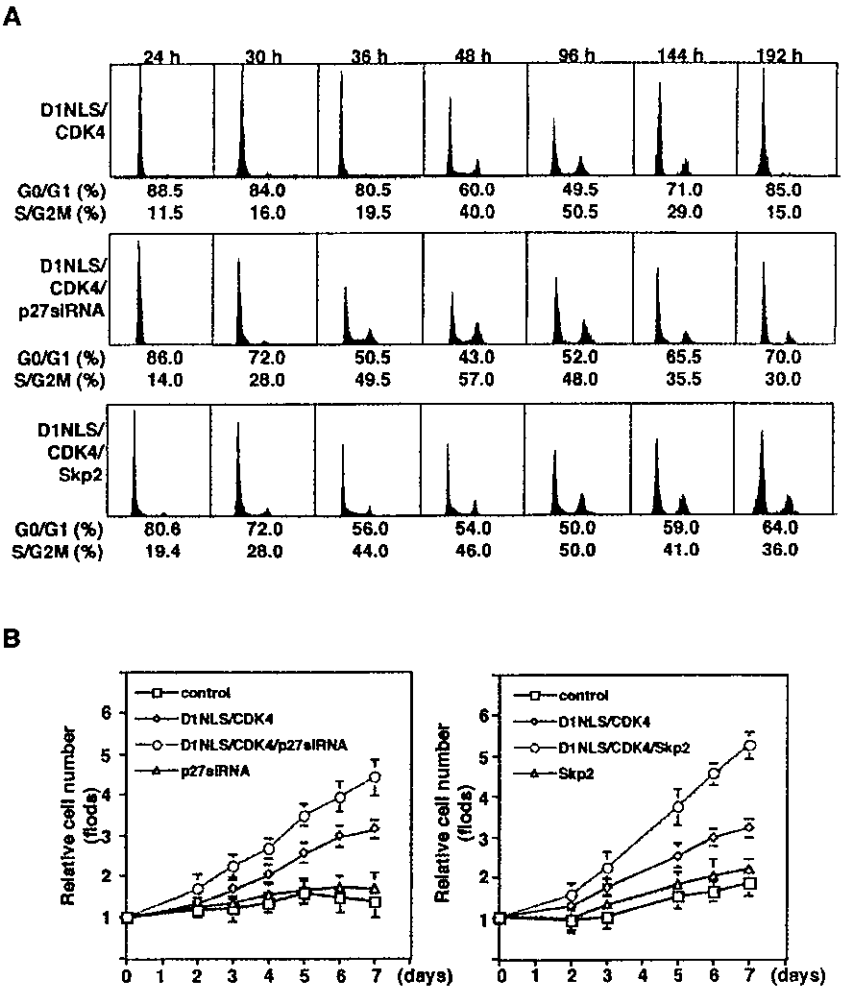

FIG. 8. **p27 down-regulation by siRNA or Skp2 promoted proliferation of D1NLS/CDK4 cardiomyocytes.** *A*, cells were infected with a combination of AdD1NLS/AdCDK4 along with Adp27 siRNA (*#6*) or AdSkp2. At each time indicated, cells were harvested and subjected to laser scanning cytometer analysis as described under "Experimental Procedures." *B*, cardiomyocytes were untreated or infected with a combination of AdD1NLS, AdCDK4, Adp27siRNA (*#6*), or AdSkp2 as indicated and cultured. Cell number was counted on the indicated day after infection, and the relative cell proliferation was expressed as mean ± S.E. of three independent experiments.

ported by the following findings, (i) *in vitro* p27 ubiquitylation activity of cell extracts or the Skp2 immunocomplex was remarkably suppressed in cardiomyocytes compared with proliferating REF52 fibroblasts (Fig. 4, *B* and *C*); (ii) p27 accumulation was observed in the nuclei of D1NLS cells (Fig. 2); (iii) p27 in serum-starved cardiomyocytes and REF52 cells exhibited apparently similar kinetics of degradation after serum stimulation (Fig. 3), suggesting no apparent difference of the Skp2-independent degradation between these cells. (iv) Skp2 protein was actively ubiquitylated in cardiomyocytes compared with REF52 cells (Fig. 5*D*). Thus, it is strongly argued that increased Skp2 degradation is one of the mechanisms by which cardiomyocytes accumulated p27 in the nuclei and ceased to grow early after the forced cell cycle progression by nuclear cyclin D1.

Other cell cycle inhibitors, p21 and p57, are also recognized and degraded by the Skp2-dependent pathway (25, 26). After cell cycle entry of cardiac cells as well as REF52 cells, p21 was also up-regulated (Fig. 1*B*). However, it was not significantly associated with CDK2 (Fig. 1*C*). Furthermore, p21 degradation in Skp2-expressed cells was less than p27, and p57 was neither induced nor affected significantly by Skp2 expression (Fig. 6*A*). Thus, we speculate it is unlikely that these inhibitors play a major role in cell cycle arrest of D1NLS cardiomyocytes. Inconsistent with this, the knockdown of p27 using the siRNA approach promoted the proliferation of D1NLS/CDK4 cells, indicating that p27 rather than p21 or p57 played a role in causing cell cycle arrest. It is interesting to note here that p27 is highly accumulated with concomitant reduction of cell growth in Skp2-deficient cells (23). In these mice, however, cardiac size or cell number was not significantly affected. In contrast, p27 knockout mice show the enlarged heart with much higher proliferative activity (21). These are consistent with our findings that Skp2 and p27 are reciprocally regulated and the specific p27 down-regulation by siRNA or Skp2 enhanced the proliferation of D1NLS/CDK4 cells. The role of cyclin kinase inhibitors p27, p21, or p57 in suppressing cell cycle progression might depend on the cell type and cellular context. Indeed, it is reported that the expression of these inhibitors in tissue is not uniform (27–29). Thus, more investigation might reveal the functional implication of these inhibitors in cell cycle arrest of terminally differentiated cells.

Cyclin E, which is a component of the late G_1 cyclin kinase CDK2 and is also recognized by Skp2 (23, 30), appeared to be regulated in a biphasic manner. It was up-regulated at low expression of Skp2, but down-regulated at a higher level of Skp2 (Fig. 6*A*). The up-regulation of cyclin E might support cell cycle progression of D1NLS/CDK4/Skp2 cells, whereas its down-regulation at the higher Skp2 level might cause another barrier for cell cycle progression. This is also an another issue of future study.

The heart is developed at the early stage of embryogenesis during which cardiomyocytes retain the ability to proliferate, but they lose the capacity to proliferate in terminal differentiation. Our present study raises an interesting possibility that the down-regulation of Skp2 by increased degradation might be

causally related to the loss of proliferation of cardiomyocytes during terminal differentiation. Inconsistent with this, we observed that fetal rat cardiomyocytes, which decrease cell growth capacity but are still capable of proliferating, exhibited the intermediate activity of the *in vitro* Skp2 ubiquitylation and p27 expression between neonatal cardiac cells and REF52 fibroblasts.[2] More recently, it has been reported that Skp2 and its cofactor Cks1 proteins are degraded by the ubiquitin ligase APC/Ccdh1 (anaphase-promoting complex/cyclosome and its activator Cdh) (31, 32). Detailed analysis of APC expression and its Skp2 degrading activity in cardiomyocytes may clarify the mechanism of terminal differentiation and such an investigation is now in progress.

Finally, we demonstrated that p27 is a strong cell cycle barrier of terminally differentiated cardiomyocytes, and its down-regulation by a combination of p27 siRNA or Skp2 and D1NLS/CDK4 significantly overrode the limited cell proliferation of cardiac cells. The impaired Skp2/p27 regulation may represent one of the molecular mechanisms by which not only cardiomyocytes but also other terminally differentiated cells lose the capacity to proliferate.

REFERENCES

1. MacLellan, W. R., and Schneider, M. D. (2000) *Annu. Rev. Physiol.* **62,** 289–319
2. Chien, K. R., and Olson, E. N. (2002) *Cell* **110,** 153–162
3. Pasumarthi, K. B., and Field, L. J. (2002) *Circ. Res.* **90,** 1044–1054
4. Olson, E. N., and Schneider, M. D. (2003) *Genes Dev.* **17,** 1937–1956
5. Orlic, D., Hill, J. M., and Arai, A. E. (2002) *Circ. Res.* **91,** 1092–1102
6. Beltrami, A. P., Barlucchi, L., Torella, D., Baker, M., Limana, F., Chimenti, S., Kasahara, H., Rota, M., Musso, E., Urbanek, K., Leri, A., Kajstura, J., Nadal-Ginard, B., and Anversa, P. (2003) *Cell* **114,** 763–776
7. Kirshenbaum, L. A., Abdellatif, M., Chakraborty, S., and Schneider, M. D. (1996) *Dev. Biol.* **179,** 402–411
8. Agah, R., Kirshenbaum, L. A., Abdellatif, M., Truong, L. D., Chakraborty, S., Michael, L. H., and Schneider, M. D. (1997) *J. Clin. Investig.* **100,** 2722–2728
9. von Harsdorf, R., Hauck, L., Mehrhof, F., Wegenka, U., Cardoso, M. C., and Dietz, R. (1999) *Circ. Res.* **85,** 128–136
10. Tamamori-Adachi, M., Ito, H., Sumrejkanchanakij, P., Adachi, S., Hiroe, M., Shimizu, M., Kawauchi, J., Sunamori, M., Marumo, F., Kitajima, S., and Ikeda, M. A. (2003) *Circ. Res.* **92,** e12–e19
11. Sherr, C. J., and Roberts, J. M. (1999) *Genes Dev.* **13,** 1501–1512
12. Pagano, M., Tam, S. W., Theodoras, A. M., Beer-Romero, P., Del Sal, G., Chau, V., Yew, P. R., Draetta, G. F., and Rolfe, M. (1995) *Science* **269,** 682–685
13. Sutterluty, H., Chatelain, E., Marti, A., Wirbelauer, C., Senften, M., Muller, U., and Krek, W. (1999) *Nat. Cell Biol.* **1,** 207–214
14. Carrano, A. C., Eytan, E., Hershko, A., and Pagano, M. (1999) *Nat. Cell Biol.* **1,** 193–199
15. Montagnoli, A., Fiore, F., Eytan, E., Carrano, A. C., Draetta, G. F., Hershko, A., and Pagano, M. (1999) *Genes Dev.* **13,** 1181–1189
16. Tsvetkov, L. M., Yeh, K. H., Lee, S. J., Sun, H., and Zhang, H. (1999) *Curr. Biol.* **9,** 661–664
17. Hara, T., Kamura, T., Nakayama, K., Oshikawa, K., Hatakeyama, S., and Nakayama, K. I. (2001) *J. Biol. Chem.* **276,** 48937–48943
18. Nakayama, K. I., Hatakeyama, S., and Nakayama, K. (2001) *Biochem. Biophys. Res. Commun.* **282,** 853–860
19. Ishida, N., Hara, T., Kamura, T., Yoshida, M., Nakayama, K., and Nakayama, K. I. (2002) *J. Biol. Chem.* **277,** 14355–14358
20. Flink, I. L., Oana, S., Maitra, N., Bahl, J. J., and Morkin, E. (1998) *J. Mol. Cell. Cardiol.* **30,** 563–578
21. Poolman, R. A., Li, J. M., Durand, B., and Brooks, G. (1999) *Circ. Res.* **85,** 117–127
22. Tamamori-Adachi, M., Ito, H., Nobori, K., Hayashida, K., Kawauchi, J., Adachi, S., Ikeda, M. A., and Kitajima, S. (2002) *Biochem. Biophys. Res. Commun.* **296,** 274–280
23. Nakayama, K., Nagahama, H., Minamishima, Y. A., Matsumoto, M., Nakamichi, I., Kitagawa, K., Shirane, M., Tsunematsu, R., Tsukiyama, T., Ishida, N., Kitagawa, M., Nakayama, K. I., and Hatakeyama, S. (2000) *EMBO J.* **19,** 2069–2081
24. Yokota, T., Sakamoto, N., Enomoto, M., Tanabe, Y., Miyagishi, M., Maekawa, S., Kurosaki, M., Taira, K., Watanabe, M., and Mizusawa, H. (2003) *EMBO Rep.* **4,** 602–608
25. Bornstein, G., Bloom, J., Sitry-Shevah, D., Nakayama, K., Pagano, M., and Hershko, A. (2003) *J. Biol. Chem.* **278,** 25752–25757
26. Kamura, T., Hara, T., Kotoshiba, S., Yada, M., Ishida, N., Imaki, H., Hatakeyama, S., Nakayama, K., and Nakayama, K. I. (2003) *Proc. Natl. Acad. Sci. U. S. A.* **100,** 10231–10236
27. Zhang, P., Wong, C., DePinho, R. A., Harper, J. W., and Elledge, S. J. (1998) *Genes Dev.* **12,** 3162–3167
28. Dyer, M. A., and Cepko, C. L. (2001) *J. Neurosci.* **21,** 4259–4271
29. Nagahama, H., Hatakeyama, S., Nakayama, K., Nagata, M., Tomita, K., and Nakayama, K. I. (2001) *Anat. Embryol.* **203,** 77–87
30. Yeh, K. H., Kondo, T., Zheng, J., Tsvetkov, L. M., Blair, J., and Zhang, H. (2001) *Biochem. Biophys. Res. Commun.* **281,** 884–890
31. Bashir, T., Dorrello, N. V., Amador, V., Guardavaccaro, D., and Pagano, M. (2004) *Nature* **428,** 190–193
32. Wei, W., Ayad, N. G., Wan, Y., Zhng, G-J., Kirschner, M. W., and Kaelin, W. G., Jr. (2004) *Nature* **428,** 194–198

[2] K. Nobori, M. T-Adachi, and S. Kitajima, manuscript in preparation.

Artificial Organs
29(2):95–103, Blackwell Publishing, Inc.
© 2005 International Center for Artificial Organs and Transplantation

A New Method for Manufacturing Cardiac Cell Sheets Using Fibrin-Coated Dishes and Its Electrophysiological Studies by Optical Mapping

*Yuji Itabashi, *Shunichiro Miyoshi, *Haruko Kawaguchi, *Shinsuke Yuasa, *Kojiro Tanimoto, *Akira Furuta, †Tatsuya Shimizu, †Teruo Okano, *Keiichi Fukuda, and *Satoshi Ogawa

**Cardiopulmonary Division, Department of Internal Medicine, Keio University School of Medicine, Shinanomachi; and †Institute of Advanced Biomedical Engineering and Science, Tokyo Women's Medical University, Kawada-cho, Shinjuku-ku, Tokyo, Japan*

Abstract: We developed a novel simple method for making functional myocardial cell sheets that may be used as transplants. Polymerized human fibrin-coated dishes were prepared with fibrinogen monomers mixed with thrombin. Neonatal rat cardiomyocytes cultured on these dishes formed myocardial cell sheets within 4 days. These cell sheets were easily dissociated intact from the polymerized fibrin layer, because the fibrin had been digested by intrinsic protease. Two overlaid myocardial cell sheets exhibited synchronized spontaneous beating and captured artificial pacing. Optical mapping confirmed that the conduction of the action potential between two partially overlaid myocardial cell sheets was established, and the action potential propagated across the junction without any delay. Transplanted three-layered myocardial cell sheets exhibited strong spontaneous beating and showed well-differentiated striations and an increase in cell size. This simple method of cell sheet engineering may also be applicable for various other cell types. **Key Words:** Tissue engineering—Cell sheet—Polymerized fibrin—Cardiomyocyte—Optical mapping—Electrical connection.

The use of organ transplantation, a powerful treatment for patients with severely damaged organs, remains limited by the shortage of donors. Recent advances in the field of regenerative medicine now promise possible alternative sources of organ grafts. The regeneration of cardiomyocytes from various stem cells, such as embryonic stem cells (1,2) and bone marrow-derived stem cells (3,4), has been observed in vitro, and a number of cell transplantation therapies have restored the function of damaged cardiac tissues. A clinical trial involving the myocardial injection of autologous myoblasts has produced a limited but important recovery of impaired cardiac function (5,6). However, the direct delivery of isolated cells that were used in these studies can induce some aggregation and necrosis of the grafted cells, and it remains difficult to transplant a sufficient number of cells to significantly improve cardiac function (7,8).

The challenge in tissue engineering has been the production of functional heart grafts with a three-dimensional structure. To maintain the three-dimensional structure of tissues, different scaffolds composed of extracellular matrix and artificial polymers have been tested (9–13). Okano et al. described a unique cell-manipulation technique that could be used to construct three-dimensional myocardial tissues by layering two-dimensional cell sheets. To obtain myocardial cell sheets, they created temperature-sensitive culture dishes by grafting temperature-responsive polymer (poly-N-isopropylacrylamide; PIPAAm) onto the surface of the dish. At 37°C, the surface is hydrophobic, and cells can attach to the dishes. However, when the temperature is dropped to 32°C or below, the surface becomes hydrophilic and the grafted polymer rapidly hydrates. The

Received May 2004; revised July 2004.
Address correspondence and reprint requests to Dr. Keiichi Fukuda, Cardiopulmonary Division, Department of Internal Medicine, Keio University School of Medicine, 35 Shinanomachi, Shinjuku-ku, Tokyo 160-8582, Japan. E-mail: kfukuda@sc.itc.keio.ac.jp

grafted polymer changes to expand, which causes cells to detach from the surface (14,15). This enables the generation of a free, confluent, thin cell sheet just by cooling the dishes to room temperature. Moreover, in contrast to enzymatic digestion, both adhesive proteins and cell–cell junctions between the confluent cells are perfectly preserved with this method, enabling generation of a three-dimensional functional tissue that lacks any scaffold.

We have developed a very simple new cell sheet engineering method using thin biodegradable polymerized fibrin-coated dishes. Here, we describe this new tissue engineering technique, and the histological and electrophysiological characteristics of the myocardial cell sheets. Electrical disconnection between the myocardial cell sheets or between a myocardial cell sheet and a host cardiac tissue may cause fatal arrhythmias (16), so we evaluated the electrical synchronization of engineered myocardial tissue with a high-resolution optical mapping system using a voltage-sensitive dye.

MATERIALS AND METHODS

Preparation of myocardial cell sheets

All experimental procedures and protocols were approved by the Animal Care and Use Committee of Keio University and conformed to the National Institutes of Health Guide for the Care and Use of Laboratory Animals. Tissiel was purchased from Baxter (Vienna, Austria), and its constitution was changed to 90 mg of human fibrinogen, 20 mg of human serum, 0.4 U of thrombin, 0.59 mg of $CaCl_2$ ($2H_2O$), and 3000 U of aprotinin. The solution was diluted with 16 mL of saline, and 0.3 mL was spread rapidly onto 35-mm culture dishes (Becton Dickinson and Company, Bedford, MA, U.S.A.). Two hours later, the polymerized fibrin-coated dishes were obtained, and they were stored at 4°C. Primary cultures of cardiomyocytes were prepared from the ventricles of 1 day-old neonatal Wistar rats (Japan CLEA, Tokyo, Japan) as described previously (17) and were plated on the dishes ($2.8 \times 10^5/cm^2$).

Transplantation of myocardial cell sheets onto adult rat subcutaneous space

The dorsal skin of male F344 nude rats (Japan CLEA) (8 weeks of age, $n = 10$), which were anesthetized by inhalation of diethyl ether (Wako, Osaka, Japan) and subcutaneous injection of 1% procaine-HCL (5–10 mL) (AstraZeneca, London, U.K.), was cut and opened. Then, trilayered myocardial cell sheets were transplanted into the subcutaneous tissue.

Histological analysis

Immunostaining was performed as described previously (18) by using antifibrin (Monosan, Uden, the Netherlands), anti-α-actinin (Sigma, St. Louis, MO, U.S.A.) monoclonal antibodies, and anticonnexin43 (Sigma) polyclonal antibodies. The samples were incubated with either Alexa488-labeled antimouse IgG antibody (Molecular Probes, Eugene, OR, U.S.A.), TRITC-labeled antirabbit IgG antibody (Dako, Tokyo, Japan) or Alexa594-conjugated phalloidin (Molecular Probes Europe BV, Leiden, the Netherlands). Nuclei were stained with TOTO-3 (Sigma). They were observed under confocal laser microscope (LSM510, Carl Zeiss International, Jena, Germany).

Electro-optical analysis of the myocardial cell sheets

For analysis of electrical communication, two myocardial cell sheets were overlapped by 2 mm at the edges and cocultured for 1, 2, and 3 days on culture dishes pretreated with laminin (Roche, Mannheim, Germany) as described previously (19). Extracellular electrical potentials at both ends of each sheet were recorded with a pair of contact bipolar electrodes. The optical mapping system was applied by using a membrane voltage indicator, di-4-ANEPPS (Molecular Probes), to monitor two-dimentional action potential propagation and the electrical connection between the two cocultured myocardial cell sheets. Di-4-ANEPPS stock solution (20 mM) was freshly prepared with DMSO (Sigma) solution containing 20% pluronic F-127 (P-3000, Molecular Probes) and added to the culture media to give a final concentration of 10 μM di-4-ANEPPS. The samples were exposed to the dye at 37°C for 30 min. The plates were then washed in Tyrode's solution consisting of (in mM) 140 NaCl, 4 Cl, 0.5 $MgCl_2$, 1.8 $CaCl_2$, 5 HEPES, 55 D-glucose (pH adjusted to 7.4 with NaOH), and 100 mg/L bovine serum albumin (Sigma). Glucose was then added to adjust the osmotic pressure of Tyrode's solution to the culture media. The myocardial cell sheets were kept in an originally made temperature-controlled chamber (37°C) on the fluorescence microscope (BX50WI, Olympus, Tokyo, Japan). Signals were monitored through a high-resolution CCD-camera system (MiCAM01, 192 × 128 points, 3.5 ms time resolution, Brain Vision, Tokyo, Japan) at an emission wavelength of greater than 610 nm and an excitation wavelength of 520 nm. The sheets were immobilized by cytochalasin-D (25 μM) (Sigma). Action potentials were observed in the case of spontaneous excitation or bipolar pacing via the contact Ag–AgCl electrode. The obtained data were processed accord-

ing to the original procedure (20) using commercial Igor Pro software (Wavemetrics, Inc., Lake Oswego, OR, U.S.A.).

RESULTS

Generation of myocardial cell sheets

The primary cell cultures contained approximately 78% desmin- and connexin43-double-positive cardiomyocytes. After the cells were plated on fibrin polymer-coated dishes (Fig. 1A,B,G), the fibrin layer was gradually degraded by proteases secreted from the cultured cells (Fig. 1C). After 4 days, the myocardial cell sheets were detached from the plates with a cell scraper (Fig. 1D,H), laid flat in culture media (medium 199/DMEM supplemented with 10% FBS) (Fig. 1E,I), then trimmed to a square shape and overlaid for subsequent experiments (Fig. 1F,J).

Histological analysis of myocardial cell sheets obtained from the polymerized fibrin-coated dishes

To assess the myocardial cell sheets obtained by this method, we collected the cells with a scraper at various time points after plating of the cardiomyocytes on the polymerized fibrin-coated dishes (Fig. 2). When the myocardial cell sheets were peeled off from the dishes after 4 days, the detached myocardial cell sheets decreased in diameter by $38 \pm 3.6\%$ ($n = 30$). Myocardial cell sheets could not be obtained by using noncoated, gelatin-, laminin-, or fibronectin-coated culture dishes (data not shown). We defined the time from the primary culture to the fabrication of the myocardial cell sheets as PX days, and the time from the fabrication to the experiment as SX days (Fig. 2A). Residual fibrin polymer was observed at the bottom of the sheet in the sample obtained on day 4 (P4–S0) (Fig. 2B), but was not detected in the sample taken on day 6 (P6–S0) (Fig. 2C). Fibrin polymer was still visible in the interstitial space in the P4–S1 sheet (Fig. 2D,F) but was completely digested in the P4–S3 sheet (Fig. 2E,G). When aprotinin (serine protease inhibitor) was added (600 KIU/mL) to the samples after separation of the cell sheets, a considerable amount of fibrin polymer was observed to have remained undigested (Fig. 2H–K).

Characteristics of the myocardial cell sheet made using the fibrin-coated dish

To investigate the optimal time to harvest the myocardial cell sheets after primary culture, we collected the cells with a scraper at various time points after plating the cardiomyocytes on the polymerized fibrin-coated dishes ($n = 12$ each, Fig. 3A). The

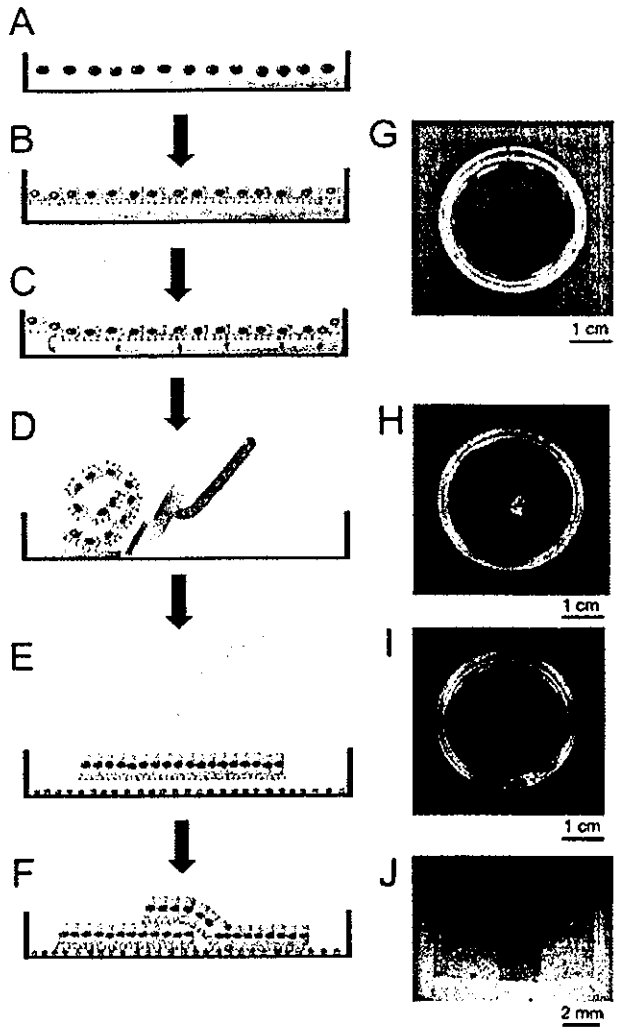

FIG. 1. Representative schema of the manipulation of myocardial cell sheets using polymerized fibrin-coated dishes. (A) Primary cultured neonate rat cardiomyocytes were spread onto the polymerized fibrin-coated dishes. (B,G) Cardiomyocytes became confluent. (C) In 4 days, the fibrin polymer had been degraded by proteases secreted from cardiomyocytes. (D) Cells were gently raked from the edge toward the center of the dishes so as not to tear the myocardial cell sheets with the cell scraper. (H) Shrunken myocardial cell sheets were obtained. (E,I) A few drops of culture media were applied to the shrunken sheets to unfold them. (F,J) The edges of the flattened myocardial cell sheets were trimmed into a square shape by using a blade. In some experiments, two myocardial cell sheets were overlaid at the margin with 2-mm width and co-cultured on laminin-coated culture dishes.

success rate for obtaining myocardial cell sheets increased after 3 days and peaked at day 4 (100% success rate).

The percentage of spontaneous beating of the myocardial cell sheets was then taken at different time intervals ($n = 12$ each). We first altered the duration of PX days while keeping SX days fixed to 3 (S3 day). The percentage of beating myocardial cell

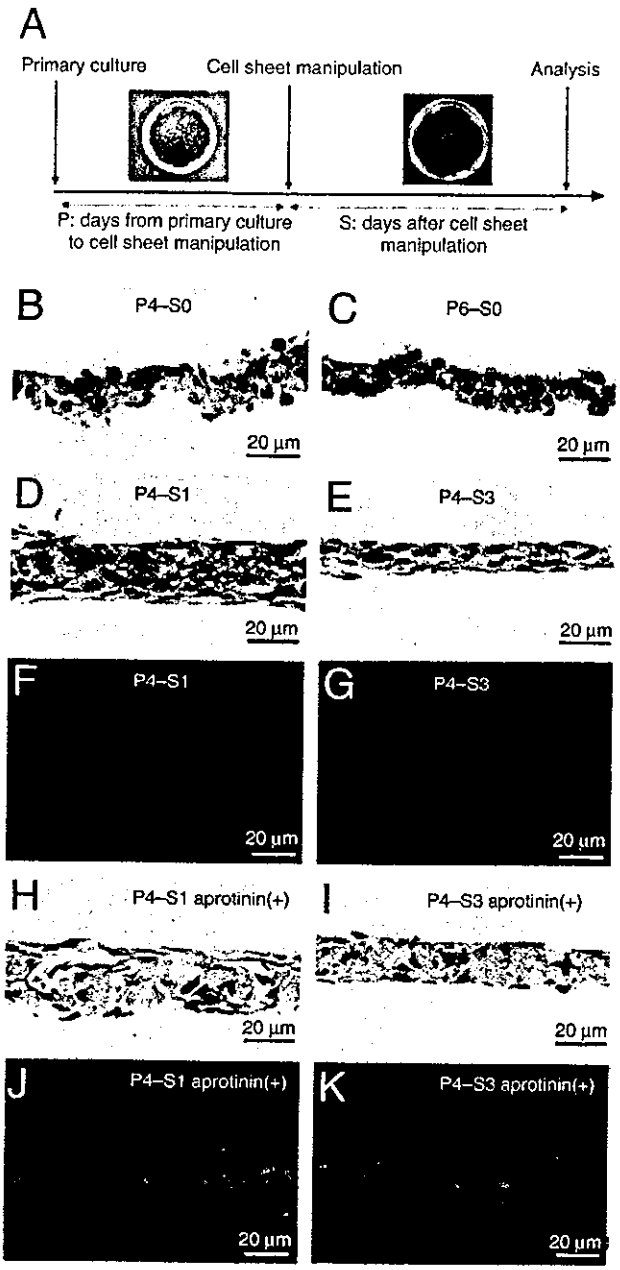

FIG. 2. Histological analysis of the myocardial cell sheets. (A) Protocol for making the myocardial cell sheets and definition of PX and SX days. (B–E,H,I) Hematoxylin and eosin staining of the myocardial cell sheets. (F,G,J,K) Immunofluorescent staining of the myocardial cell sheets. Red: F-actin; Green: fibrin; Blue: TOTO-3 indicating nuclei. Protocols and scale bars are indicated in the figure inset.

sheets showed that the difference in PX days did not affect the percentage (Fig. 3B).

Next, we fixed the PX to 4 days (P4 day), changed the length of SX days, and again measured the percentage of spontaneous beating of the cell sheets ($n = 30$). The percentage of spontaneous beating began to increase significantly from S2 day and reached 100% at S6 day (Fig. 3C). Furthermore, the percentage of myocardial cell sheets that captured artificial pacing increased from S2 day and reached 100% at S5 day (Fig. 3D).

Figure 3(E) shows the beating rate of the myocardial cell sheets from S0 day. It increased rapidly to S3 day and continued to increase at a slower rate thereafter ($n = 6$).

Inasmuch as we could reach 100% of the success rate on P4 day and P5 day, and responsiveness to artificial pacing increased remarkably for the first 3 days, the P4–S3 sheet appeared to have established relatively stable electrical nature.

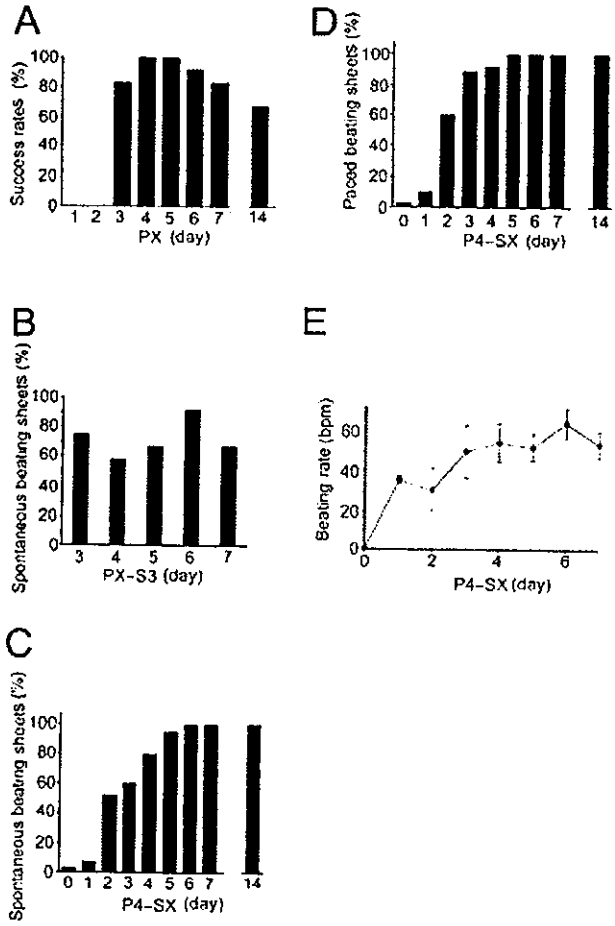

FIG. 3. Characterization of the myocardial cell sheets. Abbreviations in the figures (PX, PX–S3, P4–SX) were explained at Fig. 2(A). (A) Rate of success of obtaining myocardial cell sheets in the PX day sample. (B) Percentage of spontaneously beating myocardial cell sheets in the PX–S3 day samples. (C) Percentage of spontaneously beating sheets in the P4–SX day samples. (D) Percentage of myocardial cell sheets that captured artificial pacing in the P4–SX day samples. (E) The rate of beating in the P4–SX day samples. Values are presented as mean ± SEM.

Comparison of optical mapping with contact bipolar electrodes to analyze action potential propagation

We examined the action potential propagation within the myocardial cell sheets to determine whether an electrical connection was established between the two myocardial cell sheets. Recordings of extracellular electrical potentials at both ends of the sheets using a pair of contact bipolar electrodes were compared with the data obtained using the optical mapping system. With the use of bipolar electrodes, electrical activation was detected simultaneously on sheets A and B (Fig. 4A,C). The electrical spikes in sheets A and B were synchronous, which suggested that the two myocardial cell sheets had established an electrical connection. Subsequent optical mapping (Fig. 4D) performed on the same samples (Fig. 4B) demonstrated that the action potential arose from the lower left of sheet A, conducted to the upper right before passing through the upper junction and spreading to sheet B, meaning that action potential propagation did not follow a direct route. Thus, the optical mapping system was the more effective means of electrophysiological analysis of the action potential propagation and electrical communication between the myocardial cell sheets.

Constitution process of the electrical connection between the two cell sheets

To investigate when the electrical connection between the two myocardial cell sheets was constituted, we performed optical mapping on days 1 and 3. The action potential did not propagate from one myocardial cell sheet to the other in the P4–S1 samples (Fig. 5A–C). The contour map of propagation of the action potential (Fig. 5E) revealed that the action potential was blocked at site t. These data suggested that electrical connection was not established in the P4–S1 samples.

In contrast, the action potential propagated from sheet A to sheet B without conduction delay in the P4–S3 myocardial cell sheets (Fig. 6). All P4–S3 tissue samples had sufficient electrical communication between the two myocardial cell sheets (10/10) without any delay in conduction speed.

Histological evidence of communication between two myocardial cell sheets in vitro

Immunofluorescent staining of the P4–S3 myocardial cell sheets (Fig. 7) showed that cardiomyocytes had well-organized sarcomeres, and connexin43 was localized at the junctions between cardiomyocytes. The two-layered myocardial cell sheets were approximately 15 ± 2 μm thick, and the two layers

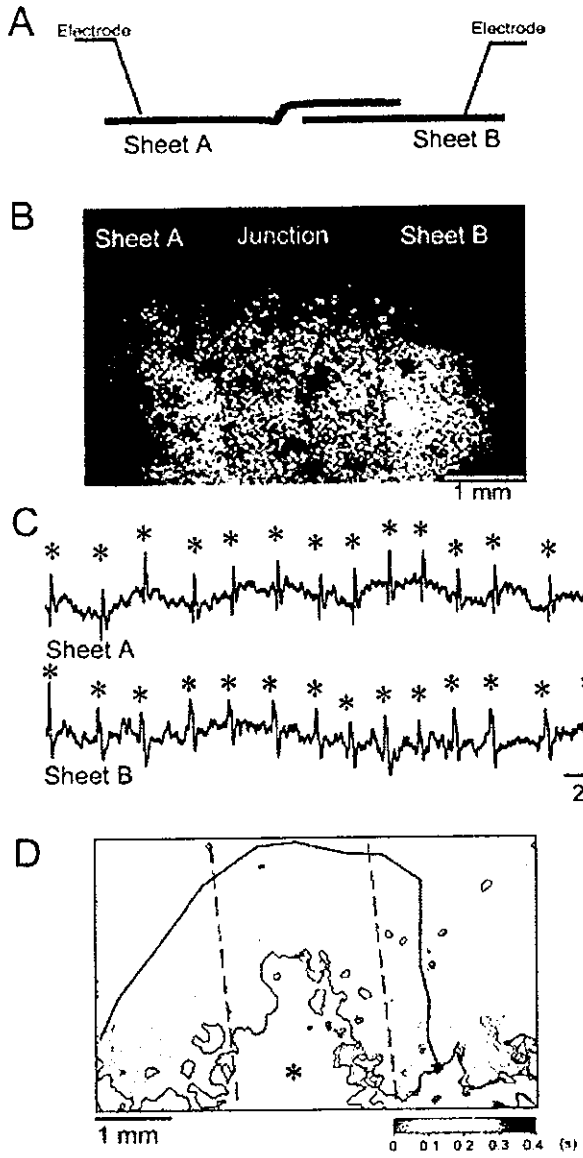

FIG. 4. Comparison of optical mapping and extracellular electrical potential recoding using a pair of contact bipolar electrodes for analysis of electrical connection between the two overlaid myocardial cell sheets. (A) Schema of the two overlaid myocardial cell sheets and position of contact bipolar electrodes, and (B) representative microscopy. (C) Extracellular electrical potentials obtained from each myocardial cell sheet, which was beating spontaneously, showing synchronization. (D) Optical image of the action potential was recorded for same sample, and an activation map was drawn from the recorded action potentials. The interval between each isochronal line was 35 ms. The spontaneous excitation originated from the left lower site of sheet A, went around the lower half of the junction which was an electrically unexcitable area (*), and propagated to sheet B via the upper half of the junction. The wave front of the action potential proceeded along the black curved line with arrowed head.

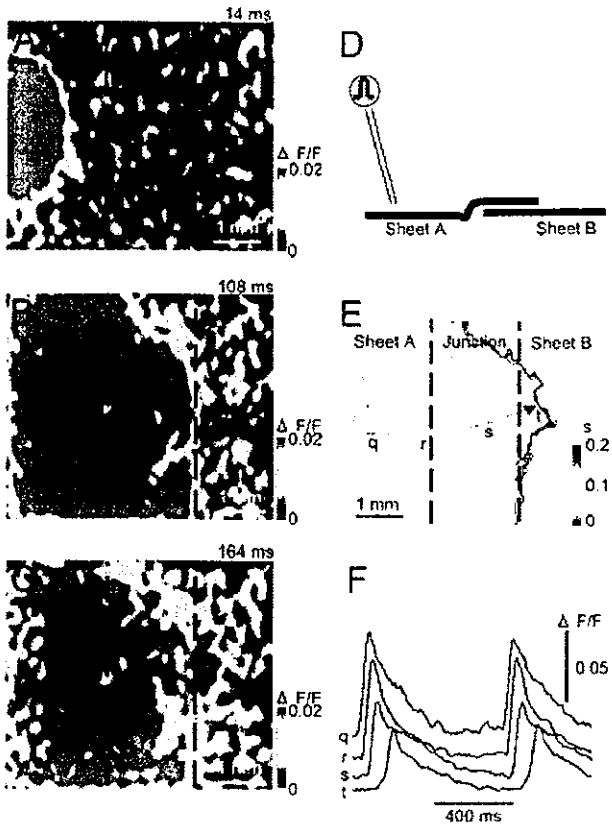

FIG. 5. Optical mapping of the action potential propagation and electrical connection of the overlaid myocardial cell sheets at day 1. Representative data at day 1. (A–C) Optical images obtained at 14, 108, and 164 ms after pacing at the left margin of sheet A, respectively. (D) Cross-sectional schematic image of the myocardial cell sheets and the site of pacing. (E) The activation map, in which the interval between each isochronal line is denoted 7 ms. There was crowding of the isochronal line at the left margin of the junction, suggesting significant conduction delay. Action potential propagation was blocked at the end of the junction. The front of the action potential proceeded along the curved line with arrowed head. (F) The action potential traces along the excitation wave front were superimposed. The character corresponds to the position of the myocyte from which the action potential was recorded.

were completely connected and indistinguishable (Fig. 7A).

Transplantation of the trilayered myocardial cell sheets in vivo

Three-layered myocardial cell sheets transplanted onto the subcutaneous tissue of nude rats showed strong rhythmical beating on posttransplant day 14 (Fig. 8A) (see supplemental Movie 3). Hematoxylin–eosin and Azan staining showed that the attached myocardial cell sheets were sandwiched between the host-derived connective tissues (Fig. 8B,C). The layers of the myocardial cell sheets were 102 ± 11 μm thick (Fig. 8E), and confocal laser microscopy showed that the length of the cardiomyocytes in vivo was greater than that of the cardiomyocytes in the cell sheets in vitro (compare Fig. 7A,B and 8E). In addition, some layers of transplanted myocardial cell sheets had rich neovascularization, not only at the capillary level but also of vessels 10–25 μm in diameter (Fig. 8D). The sarcomere of the cardiomyocytes was well organized and oriented in the same direction (Fig. 8E). These findings indicate that myocardial cell sheets obtained from the polymerized fibrin-coated dishes remained functional in vivo.

DISCUSSION

Since PIPAAm-coated dishes were first reported, significant advances have been made in cell sheet engineering of various organs, with the generation of two- and three-dimensional tissues. Cell sheet engineering has now become an important tool in the field of regenerative medicine. Cell sheets have been

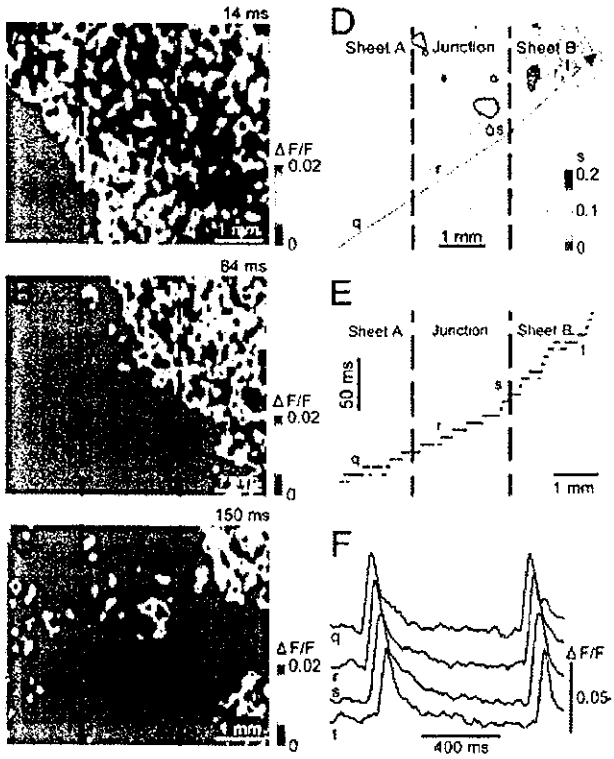

FIG. 6. Optical mapping of the action potential propagation and electrical connection of the overlaid myocardial cell sheets at day 3. Representative data at day 3. (A–C) Optical mapping images obtained at 14, 84, and 150 ms after pacing at the left margin of sheet A. (D) The calculated activation map suggested that the propagation of action potential was quite smooth with no delay between the two myocardial cell sheets. (E) The impulse propagation sequence along the excitation wave front suggested the formation of tight electrical communication between the two myocardial cell sheets. (F) The action potential traces along the excitation wave front were superimposed.

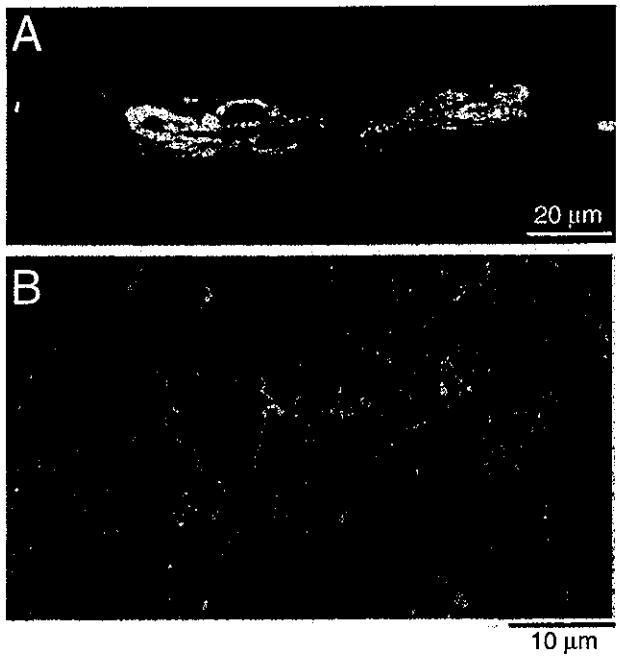

FIG. 7. Histological evidence of electrical communication between overlaid cardiomyocyte cell sheets in vitro. Laser confocal microscopy of the overlaid myocardial cell sheets (day 3), which was triple stained with antiactinin (green), anticonnexin43 (red) antibody, and TOTO-3 to stain the nucleus. (A) Side view, (B) Top view. Note that the cardiomyocytes formed a confluent sheet, and that connexin43 was clearly present at the cell junctions.

created by using temperature-sensitive culture dishes with vascular endothelial cells (14), hepatocytes (21), renal epithelial cells (22), and corneal epithelial cells.

The new method we describe here has several characteristics that were different from previous approaches using the temperature-responsive dishes. First, it does not require any specialized equipment, using only widely available fibrin polymers, nor any high level of technical expertise. Second, sheets can be generated with almost any cell type, because almost all cells will attach to polymerized fibrin-coated dishes, even those that do not attach readily to noncoated or fibronectin-coated dishes. Third, it is quick and easy to harvest the cell sheets.

Other more specialized approaches have been used to successfully generate functional tissue grafts. Li et al. used a piece of gelform, a biodegradable gelatin mesh, to form cardiac grafts from primary cultured cardiomyocytes that were transplanted into myocardial scar tissue in a cryoinjured heart (9). The cells attached to the gelatin mesh grew in three dimensions to form a beating cardiac graft, and when grafted formed cardiac tissue that contracted spontaneously. Zimmerman et al. reported that engineered heart tissue could be reconstituted by mixing cardiomyocytes from neonatal rats with liquid collagen type I, called matrigel, and that engineered heart tissue might serve as graft material to repair diseased myocardium (13). These pioneering studies, which greatly advanced research in bioengineering of cardiac grafts, both used biodegradable scaffold or collagen from other species. A scaffold can help form grafts in an appropriate shape, but they may also limit the function of the graft because of inflammation, inhibition of mechanical movement, and

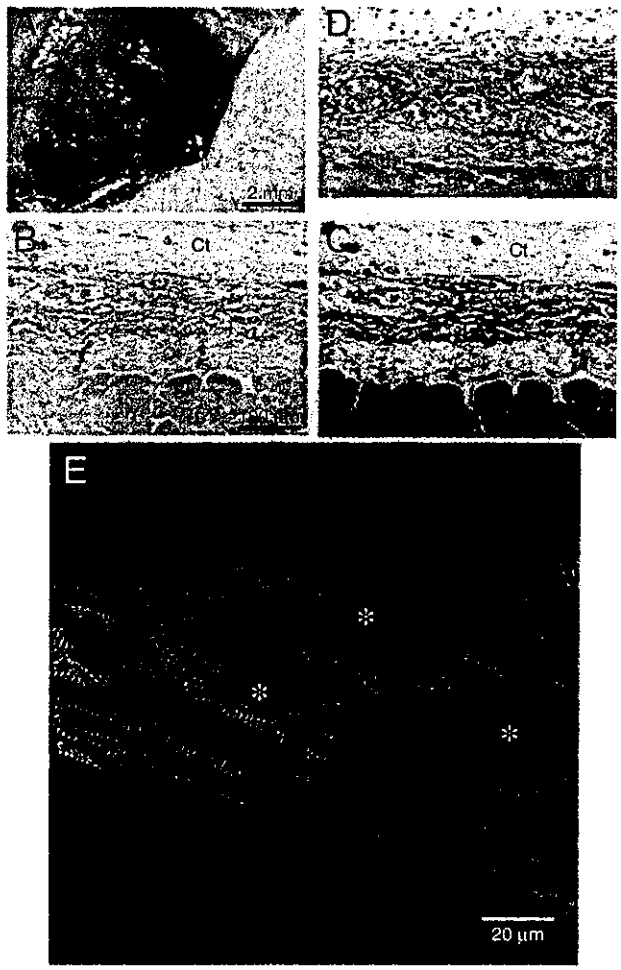

FIG. 8. Transplantation of trilayered myocardial cell sheets in vivo. The tri-layers of myocardial cell sheets were transplanted into the subcutaneous tissue of nude rats, and the samples were observed at day 14. (A) The transplanted area (black dotted line) showed rhythmical spontaneous beating (200 bpm). (B) Hematoxylin and eosin staining of the cross-sectional view of the trilayered myocardial cell sheet graft. Sk, skeletal muscle of the host rat; Ct, connective tissue; Cs, grafted trilayered myocardial cell sheets. (C) Azan staining of serial sections. (D) Note that microvessels are apparent in the grafted myocardial cell sheets. *Microvessels. (E) Triple staining of the grafted trilayered myocardial cell sheets, as described in Fig. 7. Note that the grafted cardiomyocytes show a well-organized sarcomere with a coincident direction of orientation.

adverse effects on organ function. A graft of cardiomyocytes must contract smoothly and form electrical connections with the recipient heart tissue, which a long-lived scaffold may interfere with. This is one potential advantage of our method, which has no scaffold.

We concluded that the attachment of the myocardial cell sheets to the dishes was probably loosened as fibrin was steadily degraded by proteases secreted from the grafted cardiomyocytes, as the addition of aprotinin to culture media blocked the digestion of fibrin polymers. Proteolytic degradation of fibrin probably began from the beginning of primary culture, and we observed that the residual fibrin had disappeared 6–7 days after plating of the cardiomyocytes. Loss of fibrin may vary between different cell types depending on the proteases secreted and on cell density. Plasmin is the most potent protease for fibrin in vivo, and is secreted from the liver (23). Therefore, even if the fibrin polymer remains undigested in the myocardial cell sheets after detachment from the plate, plasmin in host tissue might digest residual fibrin following transplantation. Therefore, the polymerized fibrin-coated dishes that we used provide a practical and convenient method for cell sheet engineering.

The use of a cell scraper to detach the cell sheet from the dishes did not cause any significant damage to cells. We found that cell damage at detachment was mainly dependent upon the strength of attachment of the cells to the dishes. We tested combinations of various concentrations of fibrinogen and thrombin solution and different harvest times and cell density, to find an optimal combination that left the myocardial cell sheet only very loosely attached to the dish at the time of harvest. This meant that the cell sheet could be detached with minimal cell damage or loss by just touching the margin of the dishes with a cell scraper. Moreover, in some experiments we counted the average number of cardiomyocytes in a cell sheet as 1.69×10^6 from 2.0×10^6 of primary cultured cardiomyocytes plated into a polymerized fibrin-coated dish (precise data not shown). This estimate confirmed that there was no marked loss of cells with scraping.

Finally, the conduction and propagation of action potential within and between the myocardial cell sheets is critical for successful cardiac tissue engineering. We found that measurement of P4–S3 samples by optical mapping was an effective way to evaluate conduction. This approach showed that even if the two overlaid myocardial cell sheets seemed to beat synchronously under microscopic observation, the propagation of action potential followed an indirect route via the narrowed conduction pathway. We found that 3 days are necessary to establish a sufficient electrical connection between the two myocardial cell sheets without any conduction disturbance. Thus, we think that optical mapping analysis will provide important basic data for the transplantation of myocardial cell sheets in future studies.

In the present study, we used primary cultured neonatal cardiomyocytes as the cell source, but this may not be possible for clinical use because of ethical issues. However, we hope that multipotent stem cells may, with some methodological advances, provide a sufficient source of cardiomyocytes in the near future, thereby obviating this problem.

CONCLUSIONS

We have developed a new method for generating myocardial cell sheets using polymerized human fibrin-coated dishes. Intact cell sheets of primary cultured rat cardiomyocytes were easily obtained by scraping confluent cells after the polymerized fibrin had been digested by intrinsic proteases. Two overlaid and cocultured myocardial cell sheets exhibited synchronized spontaneous beating and captured artificial pacing. Optical mapping revealed that an action potential was propagated from the junction without any delay in the two partially overlaid cell sheets. Transplanted three-layered myocardial cell sheets exhibited strong spontaneous beating, well-differentiated striations, and an increase in cell size. This technique promises to be a useful and convenient tool for generation of sheets of myocardial cells and possibly various other cell types.

Acknowledgments: This study was supported in part by research grants to K. Fukuda from the Ministry of Education, Science and Culture, Japan, and Health Science Research Grants for Advanced Medical Technology to K. Fukuda from the Ministry of Welfare, Japan. This work was performed at the Keio Integrated Medical Research Center.

REFERENCES

1. Xu C, Police S, Rao N, Carpenter MK. Characterization and enrichment of cardiomyocytes derived from human embryonic stem cells. *Circ Res* 2002;91:501–8.
2. Klug MG, Soonpaa MH, Koh GY, Field LJ. Genetically selected cardiomyocytes from differentiating embryonic stem cells form stable intracardiac grafts. *J Clin Invest* 1996;98:216–24.
3. Makino S, Fukuda K, Miyoshi S, et al. Cardiomyocytes can be generated from marrow stromal cells in vitro. *J Clin Invest* 1999;103:697–705.

4. Orlic D, Kajstura J, Chimenti S, et al. Bone marrow cells regenerate infarcted myocardium. *Nature* 2001;410:701–5.
5. Menasche P, Hagege AA, Scorsin M, et al. Myoblast transplantation for heart failure. *Lancet* 2001;357:279–80.
6. Menasche P, Hagege AA, Vilquin JT, et al. Autologous skeletal myoblast transplantation for severe postinfarction left ventricular dysfunction. *J Am Coll Cardiol* 2003;41:1078–83.
7. Muller-Ehmsen J, Peterson KL, Kedes L, et al. Rebuilding a damaged heart: long-term survival of transplanted neonatal rat cardiomyocytes after myocardial infarction and effect on cardiac function. *Circulation* 2002;105:1720–6.
8. Reinecke H, Zhang M, Bartosek T, Murry CE. Survival, integration, and differentiation of cardiomyocyte grafts: a study in normal and injured rat hearts. *Circulation* 1999;100:193–202.
9. Li RK, Jia ZQ, Weisel RD, Mickle DA, Choi A, Yau TM. Survival and function of bioengineered cardiac grafts. *Circulation* 1999;100:II63–II9.
10. Matsubayashi K, Fedak PW, Mickle DA, Weisel RD, Ozawa T, Li RK. Improved left ventricular aneurysm repair with bioengineered vascular smooth muscle grafts. *Circulation* 2003;108(Suppl 1):II219–25.
11. McDevitt TC, Woodhouse KA, Hauschka SD, Murry CE, Stayton PS. Spatially organized layers of cardiomyocytes on biodegradable polyurethane films for myocardial repair. *J Biomed Mater Res* 2003;66A:586–95.
12. Papadaki M, Bursac N, Langer R, Merok J, Vunjak-Nokavic G, Freed LE. Tissue engineering of functional cardiac muscle: molecular, structural, and electrophysiological studies. *Am J Physiol Heart Circ Physiol* 2001;280:H168–H78.
13. Zimmermann WH, Didie M, Wasmeier GH, et al. Cardiac grafting of engineered heart tissue in syngenic rats. *Circulation* 2002;106:I151–I7.
14. Kikuchi A, Okuhara M, Karikusa F, Sakurai Y, Okano T. Two-dimensional manipulation of confluently cultured vascular endothelial cells using temperature-responsive poly(N-isopropylacrylamide)-grafted surfaces. *J Biomater Sci Polym Ed* 1998;9:1331–48.
15. Shimizu T, Yamato M, Isoi Y, et al. Fabrication of pulsatile cardiac tissue grafts using a novel 3-dimensional cell sheet manipulation technique and temperature-responsive cell culture surfaces. *Circ Res* 2002;90:e40–8.
16. Rubart M, Pasumarthi KB, Nakajima H, Soonpaa MH, Nakajima HO, Field LJ. Physiological coupling of donor and host cardiomyocytes after cellular transplantation. *Circ Res* 2003;92:1217–24.
17. Kodama H, Fukuda K, Pan J, et al. Leukemia inhibitory factor, a potent cardiac hypertrophic cytokine, activates the JAK/STAT pathway in rat cardiomyocytes. *Circ Res* 1997;81:656–63.
18. Ieda M, Fukuda K, Hisaka Y, et al. Endothelin-1 regulates cardiac sympathetic innervation in the rodent heart by controlling nerve growth factor expression. *J Clin Invest* 2004:113:876–84.
19. Murata M, Fukuda K, Ishida H, et al. Leukemia inhibitory factor, a potent cardiac hypertrophic cytokine, enhances L-type Ca2+ current and [Ca2+]i transient in cardiomyocytes. *J Mol Cell Cardiol* 1999;31:237–45.
20. Koura T, Hara M, Takeuchi S, et al. Anisotropic conduction properties in canine atria analyzed by high-resolution optical mapping: preferential direction of conduction block changes from longitudinal to transverse with increasing age. *Circulation* 2002;105:2092–8.
21. Hirose M, Yamato M, Kwon OH, et al. Temperature-responsive surface for novel co-culture systems of hepatocytes with endothelial cells: 2-D patterned and double layered co-cultures. *Yonsei Med J* 2000;41:803–13.
22. Kushida A, Yamato M, Konno C, Kikuchi A, Sakurai Y, Okano T. Temperature-responsive culture dishes allow non-enzymatic harvest of differentiated Madin-Darby canine kidney (MDCK) cell sheets. *J Biomed Mater Res* 2000;51:216–23.
23. Ritchie DG, Levy BA, Adams MA, Fuller GM. Regulation of fibrinogen synthesis by plasmin-derived fragments of fibrinogen and fibrin: an indirect feedback pathway. *Proc Natl Acad Sci USA* 1982;79:1530–4.

心筋細胞の再生

Current topics and future in cardiomyocyte regeneration

林田健太郎／福田　恵一†

Kentaro Hayashida／Keiichi Fukuda†

慶應義塾大学医学部呼吸循環器内科／慶應義塾大学医学部心臓病先進治療学・講師†

Cardiopulmonary Division, Department of Internal Medicine, Keio University／Assistant Professor†, Institute for Advanced Cardiac Therapeutics, Keio University

Key Words: bone marrow, mesenchymal stem cell, cardiomyocyte, regenerative medicine, ES cell, adult stem cell, cell transplantation

Summary

Recent studies revealed that cardiomyocytes can be regenerated from both embryonic- and adult bone marrow-stem cells in animal experiment. We have established a cardiomyogenic (CMG) cell line from mouse bone marrow stromal cells that can be induced to differentiate into cardiomyocytes *in vitro* by 5-azacytidine treatment. A number of lines of evidence confirm the cardiomyocyte characteristics of CMG cells. These cells could be transplanted into the recipient heart, and survive for long period. Clinical application of these cells had some problems at present. Embryonic stem cells had ethical problems, and had a possibility of making teratoma when undifferentiated cells could not be eliminated. Adult stem cells had a difficulty in isolation and culture expansion, since they were not yet well characterized. However, transplantation of regenerated cardiomyocytes would become a future method for the treatment of severe heart failure.

Key Sentence

Recent studies revealed that cardiomyocytes can be regenerated from stem cells in animal experiment.

はじめに

従来心筋細胞は出生直後よりその増殖能を失うため，心臓は再生しない臓器と考えられていた。しかし近年における再生医学研究の目覚ましい発達により，心筋再生は実現可能なものとなりつつある。胚性幹細胞(ES細胞)や骨髄体性幹細胞を用いた心筋細胞の再生が現実のものとなり，再生心筋細胞移植により心機能が改善された，とする報告も出始めている。また幹細胞を壊死した心筋梗塞領域周辺に注入すると，心筋細胞へと分化しうることも報告されている。また，いまだ動物実験の段階ではあるものの，再生心筋細胞を利用した心不全治療への試みも始まっている。近年心臓内にも心筋幹細胞といえるような，side population(SP)細胞の存在に関する報告と，これらを用いた心筋再生による心機能の改善も報告されており，心臓再生における研究は，将来の臨床応用に向けて着実に前進しつつある。

本稿では，心臓再生の現状として現在研究されているいくつかの方法について，これらの心機能回復への応用法や問題点，さらに将来の展望について紹介していく。

I 心筋細胞再生に関する最近の話題

心筋細胞は胎生期には増殖能を有し細胞分裂を行っているが，生後まもなく最終分化してからは増殖能を失い，細胞分裂を停止すると考えられてきた。しかし近年，割合は非常に低いものの，心筋梗塞巣周囲のごく一部の心筋細胞が細胞分裂していることが報告されたため，既存の概念に対する再検討が必要となってきた[1)-4)]。この分裂像を示す細胞の性質は明らかになっていないが，あまりにわずかな細胞であり失われた心機能は代償されない。心筋細胞の増殖能を制御する研究は以前より行われてきたが，最近になって*in vitro*の実験ではあるが，細胞周期調節蛋白の1つであるcyclin D1やサイクリン依存性キナーゼCDK4の発現を制御することにより，最終分化した心筋細胞を増殖させたという報告がされ[5)]，今後の発展が期待される。

また，心臓移植後の症例の病理学的検討から興味深い報告がなされている[6)]。女性ドナーから男性レシピエントに移植された心臓に，Y染色体をもつ心筋細胞が認められた，というものである。この事実から，Y染色体をもつ心筋細胞は心臓以外の部位から幹細胞，あるいは前駆細胞として心臓に到達した，と推測されている。またヒトの骨髄移植患者4例を検討した最近の報告[7)]ではそれらの細胞の由来を骨髄と考えているが，今後さらなる検討が必要であろう。

心筋細胞の再生には幹細胞を用いる方法以外に，非心筋細胞を心筋細胞に形質転換させる方法も以前から研究されてきた。骨格筋のマスター遺伝子であるmyoDを線維芽細胞に遺伝子導入すると，その細胞が骨格筋細胞になるためのすべての遺伝子を発現し，骨格筋細胞としての性質をもつようになる。心臓でも同様なマスター遺伝子の単離が試みられてきた。心筋特異的に発現する転写因子はNkx2.5，GATA4，dHAND，eHAND，HRTなど10個以上単離されているが，マスター遺伝子は現在のところ同定されていない。

以上に挙げられた方法も試みられているが，現在最も有望であると考えられているのは，ES細

Key Sentence

Cardiomyogenic (CMG) cell line was established from mouse bone marrow stromal cells that can be induced to differentiate into cardiomyocytes *in vitro* by 5-azacytidine treatment.

胞(embryonic stem cell)や体性幹細胞を利用した心筋細胞再生であろう。

II ES細胞を用いた心筋再生

ES細胞は受精早期の胚盤胞由来の細胞で，内・中・外胚葉のいずれにも分化することができ，かつ大量に増殖することができる。ES細胞は，生体のすべての細胞に分化できる万能性幹細胞と呼ばれ，現在この細胞を用いて血液，血管内皮，神経，心筋，インスリン分泌細胞などの再生が行われている。以前からマウスでは，ES細胞を浮遊培養し，細胞を凝集させた胚様体(embryoid body)を形成させると，一部の細胞が心筋細胞となり拍動を開始することが知られていた。ヒトES細胞からもこの方法により心筋細胞が得られたと報告された[8]。

ES細胞を用いた再生にはいくつかの問題点がある。第1に，胚様体から心筋細胞が得られる確率が低く，特定の分化誘導方法が定まっていないこと。第2に，ES細胞から分化させた細胞を実際に移植する際に，未分化状態の細胞が混入すると奇形腫を形成してしまうこと。第3に，ES細胞は第三者の細胞であるため，移植後に免疫抑制剤の投与が必要となることである。以上の問題点はあるが，国内においてもヒトのES細胞作製が開始されており，さらなる発展が期待される。

III 体性幹細胞を用いた心筋再生

近年の研究により，これまで再生能をもたないと考えられていた神経や心臓にも幹細胞が存在することが明らかにされた。中胚葉由来の臓器では幹細胞は骨髄に存在すると考えられている[9]が，骨髄は元来造血の場であり造血幹細胞から血球系細胞の増殖分化が起きている。しかし，骨髄には骨髄間質細胞や造血支持細胞と呼ばれる血球系以外の細胞も存在する。骨髄間質細胞は多彩なサイトカインや細胞増殖因子を分泌し，血球系細胞の再生増殖分化を維持しており，骨芽細胞，軟骨芽細胞，脂肪細胞などに分化することが知られていた。現在では骨髄間質細胞のうち，間葉系幹細胞と呼ばれる一部の細胞が多分化能を有することが知られ，中胚葉由来の多くの細胞の幹細胞となりうると考えられている。

間葉系幹細胞は骨髄中にわずかに存在する細胞で，ヒト新生児骨髄中の細胞の10,000個に1個しか存在せず，その数は出生後急速に減少し高齢者では新生児の200分の1程度に減少するといわれている。間葉系幹細胞の同定には表面抗原が用いられているが，報告者により異なっており[10][11]，今後の研究が必要であろう。

IV 間葉系幹細胞を用いた心筋再生

われわれは骨髄間葉系幹細胞が中胚葉のさまざまな臓器の細胞に分化することより，同じ中胚葉由来の心筋細胞にも分化するのではないかと考え，間葉系幹細胞に各種の分化誘導剤を投与する実験を施行した。その結果，自己拍動をする心筋細胞に分化することを明らかにした[12]。まずマウス骨髄初代培養を行い付着系の細胞である骨髄間質細胞を分離し，長期培養することで不死化した細胞株を作製した。この多クローン細胞株にDNA脱メチル化剤である5-azacytidineを負荷しさらに2週間程度培養を続けると，非常に少ない確率ではあるが自己拍動する細胞が得られた。こ

Key Sentence

Clinical application of these stem cells had some problems at present.

の周辺の細胞を採取し同様の操作を繰り返すと，自己拍動を開始した細胞自体は継代不可能であるが心筋芽細胞と考えられる細胞は分裂，増殖を繰り返すことができる。自己拍動する割合の高いクローンを最終的にCMG(cardiomyogenesisより命名)細胞株として樹立した。CMG細胞は5-azacytidineにより最終的に分化誘導を行うと心筋細胞の表現型を獲得するが，最終分化誘導後に自己拍動を開始する比率は約30%であった。CMG細胞は培養条件下において毎分120～250程度の速さで規則的に収縮した。電顕では典型的な横紋構造に加え，心房顆粒を多数認めた。心筋細胞に分化したCMG細胞の収縮蛋白(α-アクチン，ミオシン重鎖，ミオシン軽鎖)のアイソフォームを表1に示す。心筋細胞は胎仔期，新生仔期，成獣期および心房，心室で異なる収縮蛋白のアイソフォームを示すが，CMG細胞のアイソフォームを解析すると，胎仔型心室筋に一致した表現型を取ることが明らかとなった。

ガラス微小電極によりCMG細胞の活動電位を記録すると，洞結節細胞型と心室筋細胞型の2種類が観察された(図1)。両者に共通した活動電位の特徴は，①活動電位持続時間が長いこと，②比較的浅い静止期電位をもつこと，③ペースメーカー細胞にみられる静止期電位の緩やかな脱分極が認められることであった。また，心室筋細胞型では活動電位はpeak & dome型を呈した。分化誘導後早期(2～3週間)にはすべての細胞で洞結節型が記録されたが，分化誘導後後期(4週後)には心室筋細胞型が観察され，次第に増加した。

CMG細胞の心筋細胞としての表現型を解析するため，心筋細胞特異的蛋白質の発現を調べた。CMG細胞では心房利尿ホルモンANPおよびBNPを発現していた。心筋分化に関与する転写因子としてNkx2.5, GATA4, TEF-1, eHAND, HRTなどが発現していた。MEF2 familyではMEF2A, MEF2C, MEF2Dの発現が観察された。しかし，その発現時期は3者で異なり，MEF2Cは分化誘導前で発現が認められたが，MEF2A, MEF2Dは分化誘導後に発現していた(図2)。

生体内の心筋細胞はカテコラミンα1受容体，β受容体，アセチルコリンのムスカリン受容体が発現し，心拍数や心収縮力，興奮伝導速度などの調節を行っている。CMG細胞ではα1受容体の3つのサブクラス(α1A, α1B, α1D)を発現し，α1

表1　心筋収縮蛋白のアイソフォームからみたCMG細胞の表現型

	心房筋		心室筋			CMG細胞
	胎仔型	成獣型	胎仔型	新生仔型	成獣型	
α-アクチン	skeletal	cardiac	skeletal＞cardiac	skeletal	cardiac	skeletal＞cardiac
ミオシン重鎖	α型＞β型	α型	β型＞α型	α型＞β型	α型	β型＞α型
ミオシン軽鎖	2a	2a	2v	2v	2v	2v

Embryonic stem cells had ethical problems, and had a possibility of making teratoma when undifferentiated cells could not be eliminated.

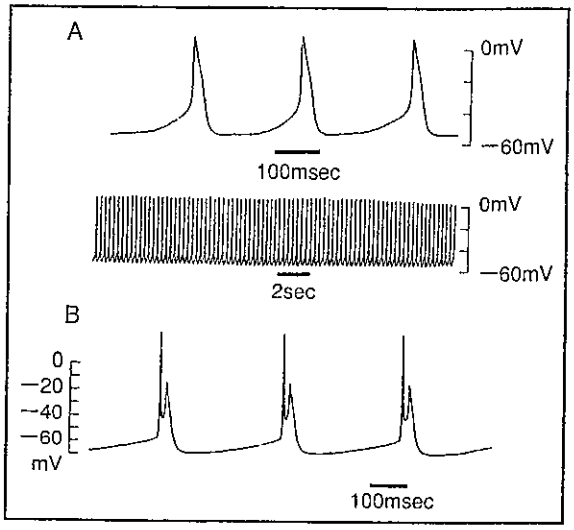

図1　骨髄由来心筋の活動電位
A：洞結節型，B：心室筋細胞型

刺激薬フェニレフリンで刺激すると，シグナルの活性化と細胞肥大が観察された[13]。一方，β受容体はβ1，β2ともに発現し，β刺激薬イソプロテレノールで刺激するとセカンドメッセンジャーのcAMPの上昇と拍動数の増加，収縮速度・収縮距離の増加が観察された。ムスカリン受容体はM1～M5まで5種類あることが知られているが，CMG細胞では本来の心筋細胞と同様にM1，M2の発現が認められ，ムスカリン受容体刺激薬カルバコールで刺激するとセカンドメッセンジャーのIP3が増加した(表2)。これらの性質はCMG細胞が心筋としての特徴をほぼ有していることを意味

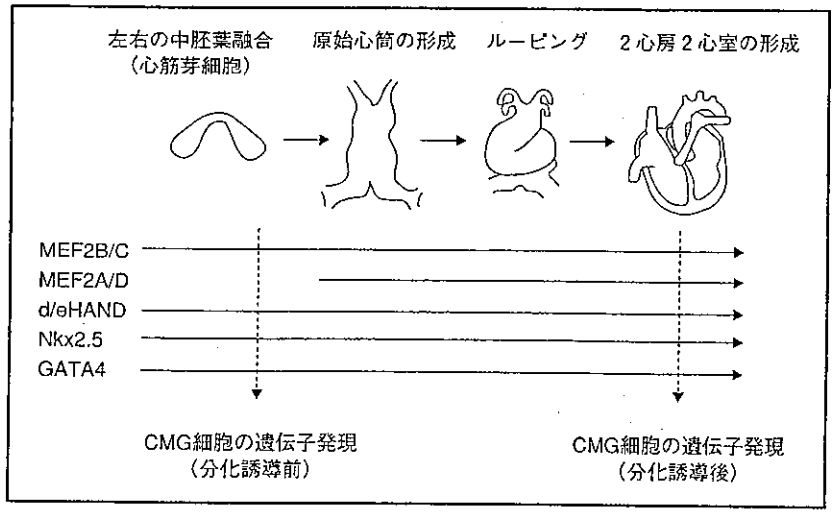

図2　心筋細胞の分化過程における転写因子の発現とCMG細胞の関係
前外側板中胚葉から心筋前駆細胞に分化した状態では，Nkx2.5, GATA4, TEF-1, HAND遺伝子などの心筋分化に必要な転写因子は発現している。CMG細胞も心筋分化に必要な遺伝子は最終分化誘導前にすでに発現していることがわかる。